Theoretical investigation of the dynamic first hyperpolarizability of DHA–VHF molecular switches†

Aurélie Plaquet,[ab] Benoît Champagne,*[a] Frédéric Castet,[b] Laurent Ducasse,[b] Elena Bogdan,[b] Vincent Rodriguez[b] and Jean-Luc Pozzo[b]

The contrast of second-order nonlinear optical response in the dihydroazulene (DHA)-vinylheptafulvene (VHF) equilibrium has been investigated as a function of the nature of the substituent (R) on the phenyl ring by means of quantum chemistry calculations including electron correlation, frequency dispersion, and solvent effects. By considering the hyper-Rayleigh scattering (HRS) response, the contrast for R = H and R = CH$_3$ between the DHA and VHF forms is larger than 5 while the contrast between the *cis* and *trans* VHF forms is close to 1. Adding the NH$_2$ donor group in *para* position of the phenyl leads to a substantial increase of the HRS first hyperpolarizability of the three forms, which is detrimental to the contrast. Then, in the case of the NO$_2$ acceptor group, a contrast is recovered because the HRS first hyperpolarizability of the DHA form is about 2–3 times larger than for both VHF forms. These variations of first hyperpolarizability as a function of the substituents as well as the associated contrasts have been explained in terms of donor/acceptor strengths and geometrical parameters.
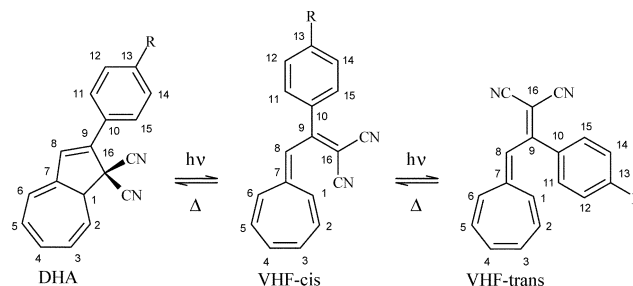
1. Introduction

Molecular switches are compounds changing their chemical and physical properties in response to external stimuli (pH, electrical current, light, temperature, pressure,…). Thanks to their remarkable properties, these systems can be employed for information processing, information storage, and communication systems. Since a few decades, several groups have investigated this field.[1] Among these investigations, a subset have concentrated on those switches that change their nonlinear optical (NLO) properties upon triggering.[2,3] The NLO response under scrutiny is the first hyperpolarizability, β, the second-order response of the electric dipole moment, μ, to an external electric field, E:

$$\mu = \mu_0 + \alpha E + 1/2\,\beta E^2 + 1/6\,\gamma E^3 + \cdots \quad (1)$$

Various photochromic compounds, including azobenzenes,[4] diarylethenes,[5] benzazolo-oxazolidines,[6] anils,[7] and spiropyrans,[8] have been studied both experimentally and theoretically with an aim of designing molecular switches with large hyperpolarizability contrasts. The strategy we have adopted in this area consists in investigating known switching species and in varying their structures by changing the aromatic and conjugated moieties as well as their substituents, following a multidisciplinary

approach that combines synthesis, experimental characterizations, and theoretical modelling.

In this paper, we investigate the dihydroazulene (DHA)–vinylheptafulvene (VHF) equilibrium by means of quantum chemistry. Indeed, the DHA–VHF systems, whose synthesis and some experimental characterizations have been reported a few years ago by Daub and co-workers,[9] present an interesting potential to display efficient NLO switching properties. In fact, the DHA–VHF system can commute between three forms: the DHA species that can undergo a photo-opening of the five-membered ring to form the VHF form in *cis* configuration, which can further be thermally converted into the VHF-*trans* form (Fig. 1). When going in the opposite direction, all transformations are thermally induced. It has been noticed that the DHA to VHF transformation is usually accompanied by a change or appearance of color depending on the substituent. In general, the DHA compounds are thermally stable, exhibit a photochromic behaviour at room temperature, display absorption bands in the UV domain, and show fluorescence in the visible region. The reaction from the DHA to the VHF forms, having at room temperature a

[a] Laboratoire de Chimie Théorique Appliquée, Facultés Universitaires Notre-Dame de la Paix (FUNDP), rue de Bruxelles 61, B-5000, Namur, Belgium. E-mail: benoit.champagne@fundp.ac.be
[b] Institut des Sciences Moléculaires – UMR 5255 CNRS – Université de Bordeaux, Cours de la Libération, 351, F-33405, Talence CEDEX, France

† Electronic supplementary information (ESI) available: Selected distances (Å) and angles (°), as calculated at the B3LYP/6-311G* level of approximation for the DHA form (Table S1), VHF-*cis* form (Table S2) and VHF-*trans* form (Table S3). See DOI: 10.1039/b900432g

Fig. 1 Photo- and thermo-chromic equilibrium for the DHA–VHF system, with atom labels used in the paper.

rather high quantum yield with values between 0.1 and 0.6, is accompanied by a large shift of the absorption band. Then, the VHF open form is metastable, non-fluorescent, and shows a high solvent dependency of the S_0–S_1 absorption transition, compared to DHA.[9a] The activation barrier for the back reaction ranges between 75 and 88 kJ mol^{-1},[9a] as a function of the substituent as well as of the polarity of the solvent: the more polar the solvent is, the faster the rearrangement is. The high quantum yield for the photochromic in DHA → VHF reaction, as well as the lack of fluorescence or photochemical back-reaction from VHF has been rationalized by Boggio-Pasqua et al. by means of complete active space-self consistent field calculations.[10] The DHA–VHF system has also been investigated by Diederich and coworkers[11] in view of elaborating three-way chromophoric molecular switches, which can be controlled by pH, light and heat. The molecule can adopt eight states by three possible switching processes, though only six have been detected.

During the photochemical ring opening of the DHA form, the electronic structure of the π-system changes considerably. Indeed, unlike in the DHA form, the cyano groups of the VHF form are conjugated with the π-system. Since this rearrangement is accompanied with a lowering of the transition energies, one can expect that it will also be accompanied by substantial modifications of the first hyperpolarizability. It is also expected that the substituent R on the phenyl ring will play an important role on the first hyperpolarizability and on its contrast. The description and rationalization of these effects for substituents R = H, CH_3, NH_2 and NO_2 are the topic of this paper. This is achieved by applying quantum chemistry approaches, which account for the effects of the solvent and include electron correlation effects. The next section summarizes the theoretical and computational aspects, section 3 presents and discusses the results on the geometrical parameters and on the nonlinear optical properties, while conclusions and outlook are drawn in section 4.

2. Theoretical and computational aspects

The geometry optimizations were carried out in vacuo and in acetonitrile at the density functional theory (DFT) level using the B3LYP exchange–correlation functional and the 6-311G* basis set. To take into account the solvent effects the Polarizable Continuum Model within the integral equation formalism (IEF-PCM)[12] was employed. We calculated the dynamic first hyperpolarizability with the Time-Dependent Hartree–Fock (TDHF)[13] scheme while the static one was obtained by using the Coupled-Perturbed Hartree–Fock (CPHF). These methods consist in expanding the matrices of the TDHF/CPHF equations in Taylor series of the external (static or dynamic) electric field and in solving these analytically order by order. However, taking advantage of the $2n + 1$ rule, only the first-order derivatives of the LCAO coefficients are needed to evaluate β. The TDHF calculations were carried out for a wavelength of 1064 nm. The reported quantities are related to the hyper-Rayleigh scattering (HRS) and electric-field induced second harmonic generation (EFISHG) experiments. In HRS experiments with plane-polarized

incident light and observation made perpendicular to the propagation plane, the full intensity reads

$$\beta_{HRS}(-2\omega; \omega, \omega) = \sqrt{\{\langle \beta_{ZZZ}^2 \rangle + \langle \beta_{XZZ}^2 \rangle\}} \quad (2)$$

whereas the depolarization ratio (DR) is given by:

$$DR = \frac{\langle \beta_{ZZZ}^2 \rangle}{\langle \beta_{XZZ}^2 \rangle} \quad (3)$$

where the $\langle \beta_{ZZZ}^2 \rangle$ and $\langle \beta_{XZZ}^2 \rangle$ terms correspond to orientational averages of all the β tensor components in the molecular frame. Full expressions for the $\langle \beta_{ZZZ}^2 \rangle$ and $\langle \beta_{XZZ}^2 \rangle$ terms can be found in ref. 8. The DR gives information on the geometry of the part of the molecule responsible for the NLO response, sometimes referred to as the NLO-phore. For a one-dimensional donor/acceptor system, DR = 5. In the case of EFISHG, the measurements give information on the projection of the vector part of β on the dipole moment vector:

$$\beta_{||}(-2\omega; \omega, \omega) = \beta_{||}$$

$$= \frac{3}{5} \sum_{\zeta}^{x,y,z} \frac{\mu_\zeta}{||\mu||} \sum_{\eta}^{x,y,z} (\beta_{\zeta\eta\eta} + \beta_{\eta\zeta\eta} + \beta_{\eta\eta\zeta})$$

$$= \frac{3}{5} \sum_{\zeta}^{x,y,z} \frac{\mu_\zeta \beta_\zeta}{||\mu||} \quad (4)$$

where $||\mu||$ is the norm of the dipole moment and μ_i and β_i the components of the μ and β vectors.

In order to estimate the electron correlation effects on the static first hyperpolarizability, we used the second-order Møller–Plesset (MP2) level in combination with the finite field procedure. To remove higher-order contaminations in the finite differentiation, the Romberg procedure was applied.[14] To account for frequency dispersion at the MP2 level, we then considered the multiplicative approximation, which consists in correcting the static MP2 values by the ratio between the TDHF and CPHF values:

$$\beta_{MP2}(-2\omega; \omega, \omega) \approx \beta_{MP2}(0; 0, 0) \times \frac{\beta_{TDHF}(-2\omega; \omega, \omega)}{\beta_{CPHF}(0; 0, 0)} \quad (5)$$

All reported β values are given in a.u. [1 a.u. of β = 3.62 × 10^{-42} m^4 V^{-1} = 3.2063 × 10^{-53} C^3 m^3 J^{-2} = 8.641 × 10^{-33} esu] within the T convention of ref. 15. All calculations were performed with the Gaussian package.[16]

3. Results and discussion

3.1 Molecular structures

A selection of remarkable geometrical parameters of the DHA, VHF-cis and VHF-trans forms calculated at the B3LYP/6-311G* level of approximation using the IEF-PCM scheme (solvent = acetonitrile) are listed in Table 1 as well as in ESI† (Tables S1–S3, where optimized geometries in the gas phase are also provided). The charges on the different fragments of the three forms obtained within Mulliken population analysis are reported in Table 2. As expected from the chemical formulas, going from DHA to VHF-cis is accompanied by a reversal of the single and

Table 1 Selection of distances (Å) and angles (°) for the DHA, VHF-*cis* and VHF-*trans* forms, as calculated at the B3LYP/6-311G* level of approximation. $BLA_1 = (d_{C_7-C_8} + d_{C_9-C_{16}} - 2d_{C_8-C_9})/2$ and $BLA_2 = (d_{C_7-C_8} + d_{C_9-C_{10}} - 2d_{C_8-C_9})/2$. Atom labels refer to Fig. 1 (See Tables S1–S3 in ESI† for more details)

	R = H	R = CH₃	R = NH₂	R = NO₂
DHA				
C_7–C_8	1.436	1.435	1.433	1.434
C_8–C_9	1.354	1.354	1.359	1.357
C_9–C_{16}	1.553	1.554	1.554	1.550
C_9–C_{10}	1.465	1.464	1.455	1.461
C_8–C_9–C_{16}	108.4	108.6	108.1	108.5
C_7–C_8–C_9–C_{16}	−5.8	−5.0	−5.7	−6.0
C_7–C_8–C_9–C_{10}	177.5	177.3	178.0	178.4
C_8–C_9–C_{10}–C_{11}	−13.8	−11.2	−11.0	−17.0
BLA_1	0.141	0.141	0.135	0.135
BLA_2	0.097	0.096	0.085	0.091
VHF-*cis*				
C_7–C_8	1.406	1.406	1.401	1.413
C_8–C_9	1.413	1.412	1.421	1.405
C_9–C_{16}	1.405	1.406	1.407	1.405
C_9–C_{10}	1.498	1.497	1.488	1.503
C_8–C_9–C_{16}	126.7	126.7	125.3	128.3
C_7–C_8–C_9–C_{16}	−29.4	−28.7	−31.8	−25.9
C_7–C_8–C_9–C_{10}	154.4	155.2	151.6	158.7
C_8–C_9–C_{10}–C_{11}	62.4	63.4	51.1	87.5
BLA_1	−0.008	−0.006	−0.018	0.004
BLA_2	0.039	0.039	0.024	0.058
VHF-*trans*				
C_7–C_8	1.407	1.406	1.401	1.409
C_8–C_9	1.412	1.413	1.422	1.408
C_9–C_{16}	1.408	1.409	1.412	1.408
C_9–C_{10}	1.491	1.488	1.473	1.493
C_8–C_9–C_{16}	120.1	119.9	119.0	120.7
C_7–C_8–C_9–C_{16}	−167.3	−165.2	−158.8	−168.9
C_7–C_8–C_9–C_{10}	17.0	19.2	25.3	16.4
C_8–C_9–C_{10}–C_{11}	57.8	54.9	44.5	58.8
BLA_1	−0.005	−0.005	−0.016	0.001
BLA_2	0.037	0.034	0.015	0.043

Table 2 Mulliken population analysis for the remarkable fragments (S₁–S₅) of the DHA, VHF-*cis* and VHF-*trans* forms as determined at the IEFPCM/B3LYP/6-311G* level of approximation. See Fig. 2 for a definition of the molecular fragments

		R = H	R = CH₃	R = NH₂	R = NO₂
DHA	S_1	+0.234	+0.011	−0.105	−0.446
	S_2	−0.106	+0.134	+0.321	+0.492
	S_3	+0.108	+0.099	+0.081	+0.126
	S_4	−0.401	−0.398	−0.409	−0.393
	S_5	+0.165	+0.152	+0.112	+0.221
VHF-*cis*	S_1	+0.231	+0.005	−0.114	−0.429
	S_2	−0.206	+0.026	+0.212	+0.385
	S_3	+0.030	+0.028	+0.031	+0.046
	S_4	−0.516	−0.522	−0.543	−0.514
	S_5	+0.462	+0.464	+0.414	+0.512
VHF-*trans*	S_1	+0.234	+0.010	−0.102	−0.424
	S_2	−0.250	−0.009	+0.191	+0.349
	S_3	+0.062	+0.065	+0.081	+0.072
	S_4	−0.527	−0.537	−0.590	−0.503
	S_5	+0.482	+0.472	+0.418	+0.507
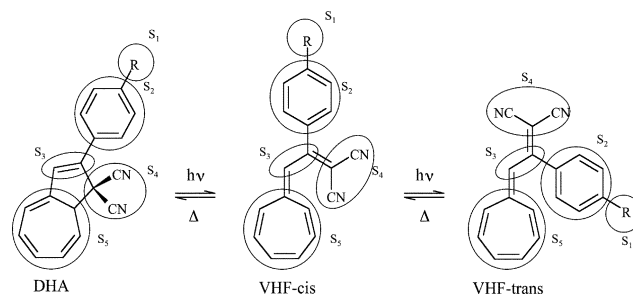
Fig. 2 Definition of the S₁–S₅ molecular fragments used in the Mulliken population analysis of the charge distribution reported in Table 2.

0.01 Å. The bond length alternation (BLA) in the central part of the molecule, defined as $BLA_1 = (d_{C_7-C_8} + d_{C_9-C_{16}} - 2d_{C_8-C_9})/2$ and $BLA_2 = (d_{C_7-C_8} + d_{C_9-C_{10}} - 2d_{C_8-C_9})/2$, decreases substantially (from 0.14 Å to −0.018/0.004 Å for BLA_1 and from 0.097/0.085 Å to 0.024/0.058 Å for BLA_2), indicating that the electron delocalization is better in VHF-*cis* than in DHA. Going from the *cis* to the *trans* form, the bond length values change little, though BLA_2 decreases by 0.002 to 0.015 Å. The largest variations are attributed to the C_9–C_{10} bond, which decreases by about 0.01 Å. This shortening of the C_9–C_{10} bond is accompanied by a lengthening of the C_9–C_{16} bond and by an increased charge transfer between the substituent R and the $C(CN)_2$ acceptor groups, in particular when R = NH₂. Moreover, the optimized DHA geometry is essentially planar with the C_7–C_8–C_9–C_{16} and C_7–C_8–C_9–C_{10} torsion angles close to 0° and 180° while the C_8–C_9–C_{10}–C_{11} torsion angle determining the position of the phenyl ring amounts to approximately 15°. Upon transition to the VHF-*cis* form, planarity is partially lost with departure from planarity of 30° (C_7–C_8–C_9–C_{16} and C_7–C_8–C_9–C_{10}), and 60° (C_8–C_9–C_{10}–C_{11}). In such a conformation, the phenyl ring is weakly conjugated with the rest of the system. Finally, the *cis*–*trans* isomerization restores a part of planarity. In particular, in the R = NH₂ case, the smaller C_8–C_9–C_{10}–C_{11} torsion angle is consistent with a partial equalization of the C_9–C_{10} and C_9–C_{16} bond lengths describing a better electron delocalization from the donor to the acceptor groups. Changing the R substituent from the NH₂ donor to the NO₂ acceptor groups has a limited impact on the geometrical parameters of the DHA form. The situation is different for the VHF forms for which one can notice variations of the C_7–C_8, C_8–C_9 and C_9–C_{10} bond lengths by 0.01–0.02 Å, leading to a (slightly) negative BLA for R = NH₂. These differences evolve monotonically with the donor or acceptor strength of the R group. Note that, changing the substituent also leads to variations of the bond lengths in the Ph ring, though small, which describe an increased quinoid character for strong donor and acceptor groups.

Mulliken population analysis (Table 2) also shows (i) the systematic decrease of the electronic density on the seven-membered ring when going from DHA to VHF, associated with π-electron delocalization in the ring and aromaticity, (ii) the transfer of most of this charge on the $C(CN)_2$ and phenyl moieties, and (iii) the mesomer D/A effects of the NH₂/NO₂

double CC bonds of the seven-membered ring whereas the changes in the phenyl ring are equal or smaller than

Table 3 Relative energies (kJ mol^{-1}) between the three forms and dipole moments (Debye) as determined at the MP2/6-31G* level of approximation taking into account the effects of the solvent with the IEFPCM scheme (solvent = acetonitrile). The geometries have been taken from the IEFPCM/B3LYP/6-311G* optimizations. The values in parentheses were obtained without accounting for the effects of the solvent in both geometry optimization and energy calculation

	R = H	R = CH$_3$	R = NH$_2$	R = NO$_2$
E(VHF-cis) − E(DHA)	33.1 (48.1)	33.1 (48.3)	33.1 (49.1)	30.9 (48.3)
E(VHF-trans) − E(DHA)	13.1 (30.0)	12.8 (29.6)	9.3 (27.1)	18.6 (33.1)
μ(DHA)	6.0	5.9	6.4	9.6
μ(VHF-cis)	11.6	11.7	10.2	14.8
μ(VHF-trans)	15.7	15.6	15.7	15.4

groups on the seven-membered ring of DHA and VHF forms when compared to R = H and R = CH$_3$.

Tables S1–S3 (ESI†) further show that the effects of the surrounding, as estimated using the IEFPCM scheme, are mostly associated with the two VHF forms and correspond to a decrease of the BLA in the bridge between the two rings. Typically, the BLA goes from −0.04/−0.05 Å to 0.00/−0.02 Å when including the effects of the solvent. This change of geometry can be associated with the important solvatochromism in VHF because the optical properties are known to depend strongly on the geometry and, in particular, on the BLA.[17]

Table 3 lists the relative energies as well as the dipole moments of the different forms as a function of the nature of the R substituent. The energy of the VHF-cis form is 31–33 kJ mol^{-1} higher than in DHA and it depends little on the nature of the substituent. When switching from the cis to the trans configuration, the VHF form is stabilized so that, in average, it is 13–14 kJ mol^{-1} higher in energy than the reference DHA form. However, the nature of the substituent has an impact on the energy difference, which goes down to 9 kJ mol^{-1} in the case of R = NH$_2$ whereas it attains 19 kJ mol^{-1} for R = NO$_2$. These variations of E(VHF-trans) − E(DHA) with the nature of R results from several effects including the increase of planarity from R = NO$_2$ to R = NH$_2$ and the reduction in BLA$_2$. Note that similar reasons could be raised for the variations of E(VHF-cis) − E(DHA) with the nature of R but that in that case, the larger dipole moment of the R = NO$_2$ compound has a supplementary stabilizing effect. If the solvent effects are not taken into account, the relative energies of the VHF forms are much larger, by about 16 kJ mol^{-1} and this difference can partly be taken into account by the increase in dipole moment between the DHA and VHF forms.

3.2 Nonlinear optical properties

Table 4 reports the first hyperpolarizabilities and the depolarization ratios evaluated at different levels of approximation *i.e.* TDHF/6-311+G* *in vacuo* and in acetonitrile, FF/MP2/6-31G* in acetonitrile, and dynamic MP2 values estimated using eqn (5). These properties have been evaluated using the geometries optimized at the IEFPCM/B3LYP/6-311G* level.

It is interesting to consider first the values calculated at the best level of approximation, *i.e.* the $\beta_{\text{MP2}}^{\text{CH}_3\text{CN}}(-2\omega;\omega,\omega)$ values.
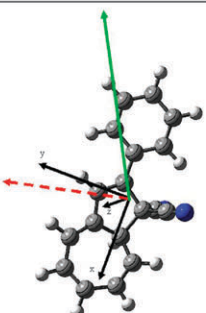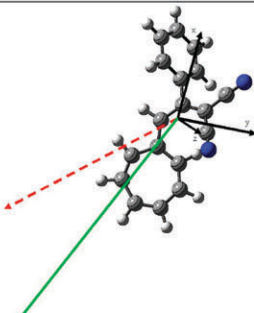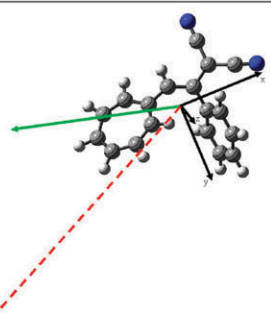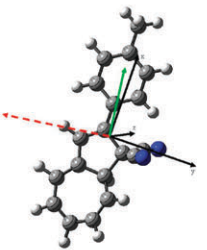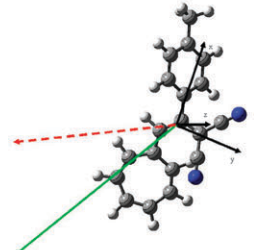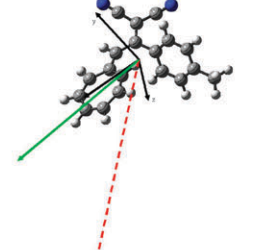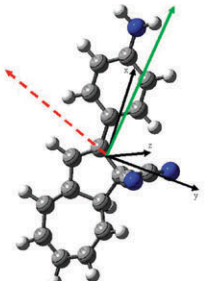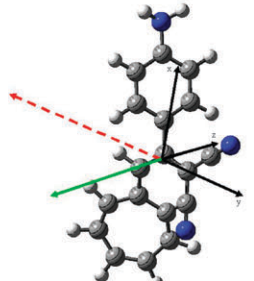
Table 4 Hyper-Rayleigh scattering quantities (β_{HRS} and DR) of DHA, VHF-cis and VHF-trans evaluated at different levels of approximation. The TDHF calculations (λ = 1064 nm) were performed using the 6-311+G* basis set while the 6-31G* was used for the FF/MP2 calculations. Dynamic MP2 values were estimated using eqn (5). All values are given in atomic units
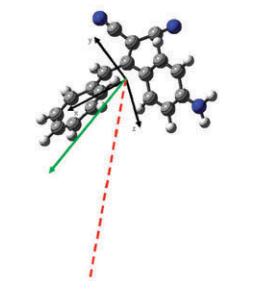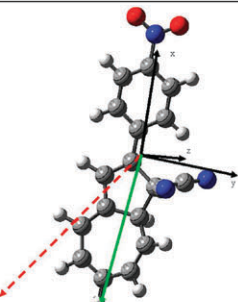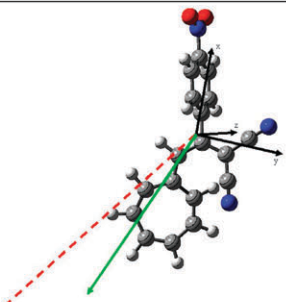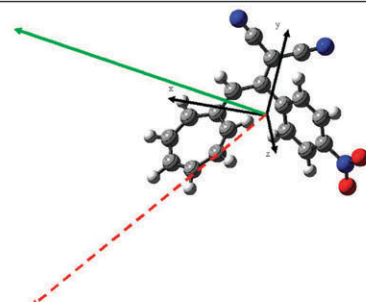
		DHA		VHF-cis		VHF-trans	
		β_{HRS}	DR	β_{HRS}	DR	β_{HRS}	DR
R = H	$\beta_{\text{TDHF}}^{vacuo}(-2\omega;\omega,\omega)$	258	5.42	1417	2.84	1623	2.39
	$\beta_{\text{TDHF}}^{\text{CH}_3\text{CN}}(-2\omega;\omega,\omega)$	229	5.11	1567	1.85	5390	3.50
	$\beta_{\text{MP2}}^{\text{CH}_3\text{CN}}(0;0,0)$	212	3.32	5973	4.55	4393	3.37
	$\beta_{\text{MP2}}^{\text{CH}_3\text{CN}}(-2\omega;\omega,\omega)$	138	—	5160	—	3466	—
R = CH$_3$	$\beta_{\text{TDHF}}^{vacuo}(-2\omega;\omega,\omega)$	743	5.25	1346	2.45	1702	2.13
	$\beta_{\text{TDHF}}^{\text{CH}_3\text{CN}}(-2\omega;\omega,\omega)$	869	5.28	1679	1.94	4916	3.08
	$\beta_{\text{MP2}}^{\text{CH}_3\text{CN}}(0;0,0)$	775	4.32	5693	4.34	5087	3.43
	$\beta_{\text{MP2}}^{\text{CH}_3\text{CN}}(-2\omega;\omega,\omega)$	704	—	4706	—	3945	—
R = NH$_2$	$\beta_{\text{TDHF}}^{vacuo}(-2\omega;\omega,\omega)$	2528	4.91	2231	2.17	2093	1.63
	$\beta_{\text{TDHF}}^{\text{CH}_3\text{CN}}(-2\omega;\omega,\omega)$	4334	4.92	4091	2.22	4176	1.57
	$\beta_{\text{MP2}}^{\text{CH}_3\text{CN}}(0;0,0)$	6320	4.93	8198	3.12	8292	3.01
	$\beta_{\text{MP2}}^{\text{CH}_3\text{CN}}(-2\omega;\omega,\omega)$	6434	—	9013	—	7055	—
R = NO$_2$	$\beta_{\text{TDHF}}^{vacuo}(-2\omega;\omega,\omega)$	2036	4.34	576	2.27	1920	2.90
	$\beta_{\text{TDHF}}^{\text{CH}_3\text{CN}}(-2\omega;\omega,\omega)$	5038	4.59	3331	4.49	7307	3.98
	$\beta_{\text{MP2}}^{\text{CH}_3\text{CN}}(0;0,0)$	5796	5.16	2075	5.09	3625	2.89
	$\beta_{\text{MP2}}^{\text{CH}_3\text{CN}}(-2\omega;\omega,\omega)$	7396	—	2583	—	3190	—

In the case of the DHA form, $\beta_{\text{MP2}}^{\text{CH}_3\text{CN}}(-2\omega;\omega,\omega)$ increases by a factor of five when going from R = H to R = Me. This enhancement is accompanied by a rotation of the β vector, which aligns itself along the *para* substitution axis of the phenyl ring, as shown in Fig. 3 in the case of the corresponding static values. $\beta_{\text{MP2}}^{\text{CH}_3\text{CN}}(-2\omega;\omega,\omega)$ is further enhanced when R = NH$_2$ and R = NO$_2$, with ratios of 47 and 54 with respect to the R = H case, respectively. Moreover, in both cases, the β vector remains aligned with respect to the *para* axis, though for R = NO$_2$, it points in the other direction, owing to its acceptor character. The substitution effects on the dipole moment amplitude and orientation are much smaller (Table 3), which can be attributed to the dominant role played by the two cyano groups. Thus, the angle between the μ and β vectors remain close to 80° for R = H, Me and NH$_2$ whereas for R = NO$_2$, the angle gets much smaller and the μ amplitude increases by about 50%.

The VHF-cis form presents a $\beta_{\text{MP2}}^{\text{CH}_3\text{CN}}(-2\omega;\omega,\omega)$ value for R = H, which is about 40 times larger than in the DHA form. On the other hand, changing the R group has a much more limited impact: with respect to R = H, $\beta_{\text{MP2}}^{\text{CH}_3\text{CN}}(-2\omega;\omega,\omega)$ decreases by 9% and 50% for R = Me and NO$_2$, respectively whereas it increases by 75% in the case of R = NH$_2$. This attributes some acceptor character to the seven-membered ring and explains the enhancement of β when it is conjugated to the amino group. Moreover, the nature of the substituent has a limited impact on the θ angle and on the orientation of the β vector with respect to the molecular frame. The situation presents some similarities for the VHF-trans form. Indeed, going from R = H to R = Me, NH$_2$ and NO$_2$, $\beta_{\text{MP2}}^{\text{CH}_3\text{CN}}(-2\omega;\omega,\omega)$ changes by +14%,

	DHA	VHF-*cis*	VHF-*trans*
R = H	β/50 θ = 73.5°	β/1000 θ = 30.1°	β/1000 θ = 41.4°
R = CH₃	β/500 θ = 95.6°	β/1000 θ = 30.1°	β/1000 θ = 37.3°
R = NH₂	β/500 θ = 71.1°	β/2000 θ = 26.9°	β/2000 θ = 26.8°
R = NO₂	β/2000 θ = 32.5°	β/500 θ = 23.2°	β/500 θ = 63.3°

Fig. 3 Sketch of the dipole moment μ (---) and first hyperpolarizability β (—) vectors for DHA, VHF-*cis* and VHF-*trans* determined at the MP2/6-31G* ($\lambda = \infty$) level of approximation. θ is the angle (in degrees) between the μ and β vectors.

+104% and −8%, respectively, whereas the θ angle remains close to 30–40°, except for R = NO₂. This change in θ is attributed to the rotation of both μ and β vectors with respect to the molecular frame. Qualitatively, these changes of orientations for μ and β are consistent with a donor character for the seven-membered ring, an acceptor character for the C(CN)₂ group, and a varying D/A character for −Ph-R as a function of the nature of R.

To address the NLO switching properties of these systems, the β_{HRS}(VHF-*cis*)/β_{HRS}(DHA) and β_{HRS}(VHF-*trans*)/

β_{HRS}(DHA) ratios were calculated. For R = H, they amount to 37.4 and 25.1, respectively, as a consequence of the very small first hyperpolarizability of the DHA form. These large contrasts do not originate from resonance effects since similar values are obtained at the static MP2 level of approximation. On the other hand, they account for the increase of π-conjugation upon going from the DHA to either of the two VHF forms, leading to an exaltation of β. When R = Me, the ratios, given in the same order, are 6.7 and 5.6. Then, for the strong donor or acceptor substituents, the ratios get much smaller, owing to the substantial increase of β_{HRS}(DHA): for R = NH$_2$, β_{HRS}(VHF-*cis*)/β_{HRS}(DHA) = 1.40 and β_{HRS}(VHF-*trans*)/β_{HRS}(DHA) = 1.10 while, for R = NO$_2$, β_{HRS}(VHF-*cis*)/β_{HRS}(DHA) = 0.35 and β_{HRS}(VHF-*trans*)/β_{HRS}(DHA) = 0.43. On the other hand, the contrast between the *cis* and *trans* forms amounts to 1.49, 1.19, 1.28 and 0.81 for R = H, Me, NH$_2$ and NO$_2$, respectively. As a conclusion, with the exception of R = NH$_2$ where the ratios are close to 1.0, the three other systems present contrasts of β at least as large as 2.3 between the DHA form and the VHF forms, demonstrating their NLO switching abilities.

The depolarization ratios also evidence modifications upon commuting between the different forms. The VHF-*trans* forms show a DR value around 3.0, quite far from the 1D reference value of 5.0. This demonstrates the non-dipolar character of this form. The DHA forms with the strong D or A groups present a DR value close to 5.0, which is in agreement with a 1D dipolar character. On the other hand, for the VHF-*cis* form, R = NO$_2$ is associated with a DR close to 5.0 whereas it is close to 3.0 for R = NH$_2$. The DR value for R = NH$_2$ is consistent with the three-branch shape of the molecule and the D/A characters of the branches whereas for R = NO$_2$, the strong acceptor character of the nitro group might overcome these of the seven-membered ring, as suggested by the orientation of the β vector in Fig. 3.

The data reported in Tables 5 and 6 enable to assess the effects of frequency dispersion and electron correlation on the HRS first hyperpolarizabilities. In acetonitrile ($\varepsilon_\omega < \varepsilon_0$), the dynamic/static ratios are close to 1.0 and, in several cases, even smaller than 1.0. In fact, these dynamic/static ratios obey the following relationships: H < Me < NH$_2$ < NO$_2$ for

Table 5 Effect of the frequency dispersion estimated from the $\beta_{\text{TDHF}}^{\text{CH}_3\text{CN}}(-2\omega;\omega,\omega)/\beta_{\text{CPHF}}^{\text{CH}_3\text{CN}}(0;0,0)$ ratio for the DHA, VHF-*cis* and VHF-*trans* forms

R	DHA	VHF-*cis*	VHF-*trans*
H	0.65	0.86	0.79
CH$_3$	0.91	0.83	0.78
NH$_2$	1.02	1.10	0.85
NO$_2$	1.28	1.24	0.88

Table 6 Effect of electron correlation estimated from the $\beta_{\text{MP2}}^{\text{CH}_3\text{CN}}(0;0,0)/\beta_{\text{CPHF}}^{\text{CH}_3\text{CN}}(0;0,0)$ ratio for the DHA, VHF-*cis* and VHF-*trans* forms

R	DHA	VHF-*cis*	VHF-*trans*
H	0.60	3.29	0.64
CH$_3$	0.81	2.80	0.80
NH$_2$	1.48	2.20	1.69
NO$_2$	1.47	0.78	0.44

Table 7 EFISHG quantities ($\beta_\parallel$) of DHA, VHF-*cis*, and VHF-*trans* evaluated at different levels of approximation. The TDHF calculations (λ = 1064 nm) were performed using the 6-311 + G* basis set while the 6-31G* was used for the FF/MP2 calculations. Dynamic MP2 values were estimated using eqn (5). All values are given in atomic units

		DHA	VHF-*cis*	VHF-*trans*
R = H	$\beta_{\text{TDHF}}^{vacuo}(-2\omega;\omega,\omega)$	−133	1218	−447
	$\beta_{\text{TDHF}}^{\text{CH}_3\text{CN}}(-2\omega;\omega,\omega)$	−171	474	−6418
	$\beta_{\text{MP2}}^{\text{CH}_3\text{CN}}(0;0,0)$	74	7269	4093
	$\beta_{\text{MP2}}^{\text{CH}_3\text{CN}}(-2\omega;\omega,\omega)$	51	−9044	3082
R = CH$_3$	$\beta_{\text{TDHF}}^{vacuo}(-2\omega;\omega,\omega)$	−101	1069	−329
	$\beta_{\text{TDHF}}^{\text{CH}_3\text{CN}}(-2\omega;\omega,\omega)$	−322	−33	−5431
	$\beta_{\text{MP2}}^{\text{CH}_3\text{CN}}(0;0,0)$	−103	6813	5069
	$\beta_{\text{MP2}}^{\text{CH}_3\text{CN}}(-2\omega;\omega,\omega)$	−89	329	3584
R = NH$_2$	$\beta_{\text{TDHF}}^{vacuo}(-2\omega;\omega,\omega)$	1276	1862	275
	$\beta_{\text{TDHF}}^{\text{CH}_3\text{CN}}(-2\omega;\omega,\omega)$	1526	3350	−1214
	$\beta_{\text{MP2}}^{\text{CH}_3\text{CN}}(0;0,0)$	2963	8697	8623
	$\beta_{\text{MP2}}^{\text{CH}_3\text{CN}}(-2\omega;\omega,\omega)$	3158	15541	2829
R = NO$_2$	$\beta_{\text{TDHF}}^{vacuo}(-2\omega;\omega,\omega)$	2355	−185	130
	$\beta_{\text{TDHF}}^{\text{CH}_3\text{CN}}(-2\omega;\omega,\omega)$	5851	−4630	−7690
	$\beta_{\text{MP2}}^{\text{CH}_3\text{CN}}(0;0,0)$	7147	2779	1849
	$\beta_{\text{MP2}}^{\text{CH}_3\text{CN}}(-2\omega;\omega,\omega)$	9497	3627	1534

DHA, H ∼ Me < NH$_2$ < NO$_2$ for VHF-*cis*, and H ∼ Me < NH$_2$ ∼ NO$_2$ for VHF-*trans*. The impact of electron correlation, as estimated from the MP2/HF ratios, is less systematic within the four substituents and within the three forms. Indeed, its effect ranges from a decrease by a factor of 2.2 to an increase by a factor of 3.3. Such a broad spectrum of MP2/HF ratios should probably draw our attention on the reliability of eqn (5), which implies similar MP2 and HF values, or rather, since we are comparing systems, similar MP2/HF ratios within a family of compounds.

In the next step, the $\beta_\parallel$ values were analyzed (Table 7, Fig. 3). Owing to the modulating effect of the θ angle, some of the ordering relationships observed for the HRS responses are not reproduced for the EFISHG quantities. Thus, for the DHA form, the EFISHG $\beta_{\text{MP2}}^{\text{CH}_3\text{CN}}(-2\omega;\omega,\omega)$ values are in the ratio 0.01 : −0.01 : 0.33 : 1.00 for R = H, Me, NH$_2$ and NO$_2$ whereas, in the same order, for the VHF-*cis* form they amount to −2.48 : 0.09 : 4.28 : 1.00 and to 2.00 : 2.33 : 1.85 : 1.00 for the VHF-*trans* form. Again, the NLO contrasts are large: for R = H, Me and NO$_2$, the three forms can be distinguished whereas for R = NH$_2$, the VHF-*cis* form displays a β values roughly five times larger than the two other forms. Though the three forms of the R = Me compound present large ratios between the first hyperpolarizabilities, the β values of the DHA and VHF-*cis* forms are small so that the practical contrast might only be visible between, on the one hand, the VHF-*trans* form and, on the other hand, the two other forms that display almost negligible β values.

Conclusions

The contrast of second-order nonlinear optical response in the dihydroazulene (DHA)–vinylheptafulvene (VHF)

equilibrium has been investigated as a function of the nature of the substituent (R) on the phenyl ring by means of quantum chemistry calculations including electron correlation, frequency dispersion, and solvent effects. By considering the hyper-Rayleigh scattering (HRS) response, the contrast for R = H and R = CH$_3$ between the DHA and VHF forms is larger than 5 while the contrast between the *cis* and *trans* VHF forms is close to 1. Adding the NH$_2$ donor group in *para* position of the phenyl leads to a substantial increase of the HRS first hyperpolarizability of the three forms, which is detrimental to the contrast. Then, for the NO$_2$ acceptor group, a contrast is recovered because the HRS first hyperpolarizability of the DHA form is about 2–3 times larger than for both VHF forms. The large first hyperpolarizability value of the R = H and R = CH$_3$ VHF forms has been attributed to the acceptor character of the seven-membered ring. For R = NO$_2$, the larger first hyperpolarizability value of the DHA form is due to the NO$_2$ attractor group, which is conjugated to the double bonds of the non-aromatic seven-membered ring whereas it decreases in the VHF-*cis* and VHF-*trans* forms as a result of the competing acceptor character of the aromatic seven-membered ring, C(CN)$_2$ and NO$_2$ groups. In the case of the electric field-induced second harmonic generation (EFISHG) response, contrasts of first hyperpolarizability are observed for the four substituents but they differ from the HRS contrasts because of the double impact of the substituent on the amplitudes and orientations of both β and μ.

Acknowledgements

References

1 (a) B. L. Feringa, *Molecular Switches*, Wiley-VCH, Weinheim, 2001; (b) F. Raymo and M. Tomasulo, *Chem.–Eur. J.*, 2006, **12**, 3186; (c) D. Gust, T. A. Moore and A. L. Moore, *Chem. Commun.*, 2006, 1169.

2 (a) B. J. Coe, *Chem.–Eur. J.*, 1999, **5**, 2464; (b) J. A. Delaire and K. Nakatani, *Chem. Rev.*, 2000, **100**, 1817; (c) B. J. Coe, *Acc. Chem. Res.*, 2006, **39**, 383.

3 (a) B. J. Coe, S. Houbrechts, I. Asselberghs and A. Persoons, *Angew. Chem., Int. Ed.*, 1999, **38**, 366; (b) I. Asselberghs, K. Clays, A. Persoons, A. M. McDonagh, M. D. Ward and J. A. McCleverty, *Chem. Phys. Lett.*, 2003, **368**, 408; (c) E. Botek, M. Spassova, B. Champagne, I. Asselberghs, A. Persoons and K. Clays, *Chem. Phys. Lett.*, 2005, **412**, 274; E. Botek, M. Spassova, B. Champagne, I. Asselberghs, A. Persoons and K. Clays, *Chem. Phys. Lett.*, 2006, **417**, 282; (d) J. F. Lamère, P. G. Lacroix, N. Farfan, J. M. Rivera, R. Santillan and K. Nakatani, *J. Mater. Chem.*, 2006, **16** 2913; (e) I. Asselberghs, G. Hennrich and K. Clays, *J. Phys. Chem. A*, 2006, **110**, 6271; (f) J. F. Lamère, P. G. Lacroix, N. Farfan, J. M. Rivera, R. Santillan and K. Nakatani, *J. Mater. Chem.*, 2006, **16**, 2913; (g) M. M. Oliva, J. Casado, J. T. Lopez Navarrete, G. Hennrich, M. C. Ruiz Delgado and J. Orduna, *J. Phys. Chem. C*, 2007, **111**, 18778; (h) M. Giraud, A. Léaustic, R. Guillot, P. Yu, P. G. Lacroix, K. Nakatani, R. Pansu and F. Maurel, *J. Mater. Chem.*, 2007, **17**, 4414; (i) V. Aubert, V. Guerchais, E. Ishow, K. Hoang-Thi, I. Ledoux, K. Nakatani and H. Le Bozec, *Angew. Chem., Int. Ed.*, 2008, **47**, 577; (j) Y. Takimoto, C. M. Isborn, B. E. Eichinger, J. J. Rehr and B. H. Robinson, *J. Phys. Chem. C*, 2008, **112**, 8016; (k) L. Boubekeur-Lecaque, B. J. Coe, K. Clays, S. Foerier, T. Verbiest and I. Asselberghs, *J. Am. Chem. Soc.* 2008, **130**, 3286.

4 R. Loucif-Saïbi, K. Nakatani, J. Delaire, M. Dumont and Z. Sekkat, *Chem. Mater.*, 1993, **5**, 229.

5 (a) S. L. Gilat, S. H. Kawaï and J.-M. Lehn, *Chem.–Eur. J.*, 1995, **1**, 275; (b) C. Bertarelli, M. C. Gallazzi, A. Lucotti and G. Zerbi, *Synth. Met.*, 2003, **139**, 933; (c) K. Higashiguchi, K. Matsuda, N. Tanifuji and M. Irie, *J. Am. Chem. Soc.*, 2005, **127**, 8922.

6 (a) L. Sanguinet, J. L. Pozzo, V. Rodriguez, F. Adamietz, F. Castet, L. Ducasse and B. Champagne, *J. Phys. Chem. B*, 2005, **109**, 11139; (b) F. Mançois, V. Rodriguez, J. L. Pozzo, B. Champagne and F. Castet, *Chem. Phys. Lett.*, 2006, **427**, 153; (c) L. Sanguinet, J. L. Pozzo, M. Guillaume, B. Champagne, F. Castet, L. Ducasse, E. Maury, J. Soulié, F. Mançois, F. Adamiez and V. Rodriguez, *J. Phys. Chem. B*, 2006, **110**, 10672; (d) F. Mançois, L. Sanguinet, J. L. Pozzo, M. Guillaume, B. Champagne, V. Rodriguez, F. Adamietz, L. Ducasse and F. Castet, *J. Phys. Chem. B*, 2007, **111**, 9795.

7 (a) K. Nakatani and J. A. Delaire, *Chem. Mater.*, 1997, **9**, 2682; (b) I. Asselberghs, Y. Zhao, K. Clays, A. Persoons, A. Comito and Y. Rubin, *Chem. Phys. Lett.*, 2002, **364**, 279; (c) M. Sliwa, S. Létard, I. Malfrant, M. Nierlich, P. G. Lacroix, T. Asahi, H. Matsuhara, P. Yu and K. Nakatani, *Chem. Mater.*, 2005, **17**, 4727; (d) M. Sliwa, K. Nakatani, T. Asahi, P. G. Lacroix, R. B. Pansu and H. Masuhara, *Chem. Phys. Lett.*, 2007, **437**, 212; (e) M. Guillaume, B. Champagne, N. Markova, V. Enchev and F. Castet, *J. Phys. Chem. A*, 2007, **111**, 9914; (f) A. Plaquet, M. Guillaume, B. Champagne, L. Rougier, F. Mançois, V. Rodriguez, J.-L. Pozzo, L. Ducasse and F. Castet, *J. Phys. Chem. C*, 2008, **112**, 5638.

8 A. Plaquet, M. Guillaume, B. Champagne, F. Castet, L. Ducasse, J.-L. Pozzo and V. Rodriguez, *Phys. Chem. Chem. Phys.*, 2008, **10**, 6223.

9 (a) H. Görner, C. Fischer, S. Gierisch and J. Daub, *J. Phys. Chem.*, 1993, **97**, 4110; (b) H. Görner, C. Fischer and J. Daub, *J. Photochem. Photobiol., A*, 1995, **85**, 217; (c) T. Mrozek, H. Görner and J. Daub, *Chem. Commun.*, 1999, 1487; (d) J. Ern, M. Petermann, T. Mrozek, J. Daub, K. Kuldová and C. Kryschi, *Chem. Phys.*, 2000, **259**, 331; (e) V. De Waele, U. Schmidhammer, T. Mrozek, J. Daub and E. Riedle, *J. Am. Chem. Soc.*, 2002, **124**, 2438; (f) V. De Waele, U. Schmidhammer, E. Riedle and J. Daub, *Chem. Phys. Lett.*, 2004, **390**, 328.

10 M. Boggio-Pasqua, M. J. Bearpark, P. A. Hunt and M. Robb, *J. Am. Chem. Soc.*, 2002, **124**, 1456.

11 L. Gobbi, P. Seiler and F. Diederich, *Angew. Chem., Int. Ed.*, 1999, **38**, 674.

12 (a) J. Tomasi and M. Persico, *Chem. Rev.*, 1994, **94**, 2027; (b) J. Tomasi, B. Mennucci and R. Cammi, *Chem. Rev.*, 2005, **105**, 2999.

13 (a) H. Sekino and R. J. Bartlett, *J. Chem. Phys.*, 1986, **85**, 976; (b) S. P. Karna and M. Dupuis, *J. Comput. Chem.*, 1991, **12**, 487.

14 H. D. Cohen and C. C. J. Roothaan, *J. Chem. Phys.*, 1965, **43**, S34.

15 A. Willetts, J. E. Rice, D. A. Burland and D. P. Shelton, *J. Chem. Phys.*, 1992, **97**, 7590.

16 M. J. Frisch, G. W. Trucks, H. B. Schlegel, G. E. Scuseria, M. A. Robb, J. R. Cheeseman, J. A. Montgomery, Jr., T. Vreven, K. N. Kudin, J. C. Burant, J. M. Millam, S. S. Iyengar, J. Tomasi, V. Barone, B. Mennucci, M. Cossi, G. Scalmani, N. Rega, G. A. Petersson, H. Nakatsuji, M. Hada, M. Ehara, K. Toyota, R. Fukuda, J. Hasegawa, M. Ishida, T. Nakajima, Y. Honda, O. Kitao, H. Nakai, M. Klene, X. Li, J. E. Knox, H. P. Hratchian, J. B. Cross, V. Bakken, C. Adamo, J. Jaramillo, R. Gomperts, R. E. Stratmann, O. Yazyev, A. J. Austin, R. Cammi, C. Pomelli, J. Ochterski, P. Y. Ayala, K. Morokuma, G. A. Voth, P. Salvador, J. J. Dannenberg, V. G. Zakrzewski, S. Dapprich, A. D. Daniels, M. C. Strain, O. Farkas, D. K. Malick, A. D. Rabuck, K. Raghavachari, J. B. Foresman, J. V. Ortiz, Q. Cui, A. G. Baboul, S. Clifford, J. Cioslowski, B. B. Stefanov, G. Liu, A. Liashenko, P. Piskorz, I. Komaromi, R. L. Martin, D. J. Fox, T. Keith, M. A. Al-Laham, C. Y. Peng, A. Nanayakkara, M. Challacombe, P. M. W. Gill, B. G. Johnson, W. Chen, M. W. Wong, C. Gonzalez and J. A. Pople, *GAUSSIAN 03 (Revision C.02)*, Gaussian, Inc., Wallingford, CT, 2004.

17 S. R. Marder, C. B. Gorman, B. G. Tiemann, J. W. Perry, G. Bourhill and K. Mansour, *Science*, 1993, **261**, 186.